Materials Today Bio 32 (2025) 101712

Contents lists available at ScienceDirect

Materials Today Bio

journal homepage: www.journals.elsevier.com/materials-today-bio

Metal–organic framework–based delivery systems as nanovaccine for enhancing immunity against porcine circovirus type 2

Luo-Gang Ding [a,b,1], Min Shi [a,b,1], Er-Di Yu [a,b], Yu-Lin Xu [a], Yu-Yu Zhang [a,b], Xing-Liang Geng [c], Fei Liu [a], Jian-Da Li [a], Zhi Chen [a], Jiang Yu [a,b,*], Jia-Qiang Wu [a,b,**]

[a] Key Laboratory of Livestock and Poultry Multiomics of MARA, Institute of Animal Science and Veterinary Medicine, Shandong Academy of Agricultural Sciences, Jina, 250100, China
[b] College of Life Science, Shandong Normal University, Jinan, 250014, China
[c] Shandong Binzhou Wohua Biotech Co., Ltd., Binzhou, 256606, China

ARTICLE INFO

Keywords:
Porcine circovirus type 2
Metal–organic framework
Delivery system
Vaccine
Immune response

ABSTRACT

Porcine circovirus type 2 (PCV2) has caused massive economic losses to the global pig farming industry. As emerging nanomaterials, metal–organic frameworks (MOFs) have considerable potential in drug and vaccine delivery because of their unique physicochemical properties. Based on the successful expression and identification of PCV2 antigens (Cap protein), this study exploits MOF platforms to design a nanovaccine delivery system (Cap@ZIF-8-CpG) as a novel subunit vaccine, which effectively enhances the resistance of antigens to denaturation and boosts immune responses against PCV2. Results demonstrate that mice injected with a nanovaccine efficiently incorporating PCV2 antigens (Cap) and an immune enhancer (CpG) elicit robust humoral immune responses. Notably, immunoglobulin G antibody titers are considerably elevated; cytokine secretion is augmented; and the proliferation of $CD8^+$ cytotoxic T lymphocytes and $CD4^+$ T cells is effectively stimulated. Following a viral challenge, the Cap@ZIF-8-CpG nanovaccine successfully protects the health of the mice, making them resistant to PCV2 infection. This study provides a new promising direction for the development of effective and long-lasting vaccines against PCV2 and other major swine pathogens.

1. Introduction

Porcine circovirus type 2 (PCV2) is a contagious and economically significant virus that poses a severe threat to the human public health and swine industry worldwide [1–5]. PCV2 was first identified in post-weaning pigs with multisystemic wasting syndrome. Thus, the disease was named postweaning multisystemic wasting syndrome (PMWS) or PCV2 systemic disease. This virus is transmitted horizontally among pigs, primarily shed in nasal secretions and saliva, and mainly transmitted via the oronasal route. Contaminated fomites are the main sources of infection [6–10]. PCV2, a member of the *Circovirus* genus within the *Circoviridae* family, is among the smallest DNA viruses, with a diameter of 16–18 nm. Its genome exhibits a compact, single-stranded, closed circular structure, ~1.7 kbs in length. Notably, approximately 10 open reading frames (ORFs) can be identified in PCV2. Among these, ORF1 and ORF2 are the primary major ORFs and arranged in head to tail opposite direction. ORF1 encodes a replicase protein weighing 35.7 kDa, which is crucial for virus replication. While ORF2 encodes the capsid protein (Cap) with molecular weight of 28–30 kDa that can self-assemble to viral like particles (VLP) [11], playing a vital role as an immunogenic protective antigen for host inducing protective immunity [12–14]. The economic impact of PCV2 infections is immense, associated with substantial mortality, morbidity, and production losses in infected herds.

At present, primary vaccination strategies against PCV2 primarily depend on inactivated or subunit vaccines [15–19]. While vaccines have demonstrated some degree of effectiveness in mitigating the prevalence of PCVAD, they often suffer limited immunogenicity, necessitating

* Corresponding author. Key Laboratory of Livestock and Poultry Multiomics of MARA, Institute of Animal Science and Veterinary Medicine, Shandong Academy of Agricultural Sciences, Jinan, 250100, China.
** Corresponding author. Key Laboratory of Livestock and Poultry Multiomics of MARA, Institute of Animal Science and Veterinary Medicine, Shandong Academy of Agricultural Sciences, Jinan, 250100, China.
E-mail addresses: yujiang@saas.ac.cn (J. Yu), wujiaqiang1@saas.ac.cn (J.-Q. Wu).
[1] L.-G. Ding, and M. Shi contributed equally to this work.

https://doi.org/10.1016/j.mtbio.2025.101712
Received 19 December 2024; Received in revised form 19 March 2025; Accepted 26 March 2025
Available online 27 March 2025

frequent booster administrations to sustain protective immunity [20–22]. Furthermore, these vaccines do not always prevent the establishment of chronic PCV2 infections, which can persist lifelong and continuously threaten the health and productivity of infected animals [23–25]. Consequently, we urgently need to develop innovative vaccine delivery systems that can enhance humoral immunity and afford long-lasting protection against PCV2 infection [26].

Metal–organic frameworks (MOFs), a class of crystalline porous nanomaterials, have emerged as promising candidates for use in drug delivery and vaccine administration because of their unique physicochemical properties [27–31]. These materials, comprising metal ions or clusters interconnected by organic ligands, exhibit exceptional porosity, vast surface areas, and adjustable pore sizes, making them ideal candidates for encapsulation and delivery of antigens or adjuvants. The long-range ordered pore structure of MOFs affords them with high loading capacity. Various units can be efficiently enriched in MOFs by adjusting the specific interactions between the chemistry of pores and guest biomolecules, facilitating functional diversification [32–34]. Furthermore, the ability to tailor MOFs at the molecular level allows for precise control over the encapsulation and release of antigens or adjuvants. This precise control ensures that antigens are efficiently delivered to immune cells, stimulating robust immune responses [35,36]. MOFs offer the possibility of precise control over the release kinetics of encapsulated cargoes. Meanwhile, the chemistry of the pore–wall surface interface and the rate of antigens released can be controlled via regulation of host–guest interactions, ensuring sustained antigen presentation and prolonged immune stimulation [37,38]. These features, combined with their remarkable biocompatibility, make MOFs promising candidates for use in vaccine delivery systems [39–41]. The ability of MOFs to efficiently enrich and deliver antigens and adjuvants/immunopotentiators to immune cells, combined with precise control over antigen release, offers notable potential for enhancing vaccine potency and immunogenicity.

Previously, PCV2 Cap expressed in Sf9 cells was found to self-assemble to virus-like particles (VLPs) and it was immunogenic [42]. Furthermore, the PCV2 VLP incorporated with CpG ODN have been demonstrated to enhance a protective immunity in immunized mice compared to VLP alone [43]. Additionally, ZIP-8-CpG has been reported to induce innate immune response in mice [44]. Based on this, we introduce a novel, MOF-based nanoscale delivery system, namely, Cap@ZIF-8-CpG, as a novel subunit vaccine for achieving enhanced immune response against PCV2. The vaccine is prepared using zeolitic imidazolate framework-8 (ZIF-8), a remarkable carrier for encapsulating the Cap protein and adsorbing the CpG immunopotentiator. Results demonstrate that the presence of ZIF-8 shells prevents internal protein degradation and enhances the antigen uptake efficiency of macrophages. Moreover, the efficient enrichment of Cap and CpG within ZIF-8 ensures rapid antigen-depot establishment at the injection site. Subsequently, the vaccine is internalized by immune cells, triggering robust antigen presentation and T-cell activation, which induces potent humoral immune responses. Further investigations demonstrate that Cap@ZIF-8-CpG substantially enhances the production of cytokines, facilitating the activation and proliferation of $CD8^+$ cytotoxic T lymphocytes ($CD8^+$ CTLs) and $CD4^+$ T cells. Furthermore, MOF-delivered antigens elicit long-lasting memory immune responses, providing sustained protection against PCV2 challenge *in vivo*. This study aims to contribute to the development of novel, safe, and effective MOF-based vaccine platforms.

2. Materials and methods

2.1. Materials and instruments

All reagents were analytical reagent grade without further purification. A complete Dulbecco's Modified Eagle Medium (DMEM) basic solution (1×) (Gibco, CA, USA) with 1.0 % (*v/v*) penicillin–streptomycin (Gibco, CA, USA) and 10 % (*v/v*) fetal bovine serum (Gibco, CA, USA) was used as the medium for cell culture. In addition, a 0.25 % trypsin–ethylenediaminetetraacetic acid solution (1×) was obtained from Gibco (USA). CpG oligodeoxynucleotides (CpG ODNs) were purchased from Sangon Biotechnology Inc.(Shanghai, China); sequence (5′-TGT ACG GGC CAG ATA TAC GCG TAA CGT CAA ACG TTA AAA CAG CGA AAC GTC AAA CGT AAA GAC GAA AAC GTC AAA ACG TTA AAA CGA CGA AAC GTC AAA CGT AAA GAC GAA AAC GTC AAA ACG TTA AAA CGA CGA AAC GTC AAA CGT TAA ACG ACG AAC GCG TTG ACA TTG A-3′). ActinRed™ 555 (Rhodamine phalloidin) and Pierce™ Bicinchoninic Acid (BCA) Protein Assay Kits were obtained from Thermo Fisher Scientific. Immunoglobulin G2a (IgG2a) and IgG1 were purchased from Jackson ImmunoResearch (PA, USA). PCV2 Antibody enzyme-linked immunosorbent assay (ELISA) detection kit was purchased from MEDIAN Diagnostics (South Korea). Mouse interleukin 2 (IL-2), IL-4, and interferon alpha (IFN-γ) ELISA scientific research kits were purchased from Jiangsu Meimian Industrial Co., Ltd (Jiangsu, China). Horseradish peroxidase (HRP)-labeled goat antimouse IgG (H + L) was purchased from Beyotime (Shanghai, China).

Fourier-transform infrared spectroscopy (FT-IR) spectra were obtained using a Bruker ALPHA spectrometer. Powder X-ray diffraction (PXRD) patterns were obtained on a D8 Advance X-ray powder diffractometer, utilizing Cu Kα radiation with a wavelength of 1.5405 Å. Scanning electron microscopy (SEM) was conducted on the Gemini Zeiss SUPRA microscope. Transmission electron microscopy (TEM) images were acquired using a Hitachi HT7700 120 kV Compact-Digital Transmission Electron Microscope. Nitrogen-adsorption isotherms were measured at 77 K on an ASAP 2020/TriStar 3000 instrument. Thermogravimetric analysis (TGA) was carried out in a flowing-nitrogen atmosphere at temperatures ranging from 25 °C to 800 °C using a TGA/DSC1-Thermogravimetric Analyzer from Mettler Toledo. Ultraviolet–visible (UV–Vis) spectroscopy was performed on a TU-1900 instrument from Beijing PuXi. Dynamic light scattering (DLS) analysis was conducted using a Malvern Zetasizer Nano ZS90 apparatus. Microplate assays were performed on a Molecular Devices SpectraMax i3x Multimode Microplate Detection System. Fluorescence images were acquired via confocal laser scanning microscopy (CLSM) using a Leica TCS SP8 system. The cellular uptake efficiency was analyzed via flow cytometry using a Beckman Coulter CytoFLEX cytometer.

2.2. Expression and purification of the Cap protein

To achieve the efficient expression of the PCV2 Cap protein, the baculovirus expression system was used. The ORF2 fragment originated from a PCV2d genotype strain (GenBank: JQ653449.1). The optimized Cap gene sequence was inserted into the baculovirus expression vector pFastBacHTB (Thermo Fisher Scientific Inc., Cat# 10359016) via *Bam*HI (TransGen Biotech, Cat# JB101-01) and *Xho*I (TransGen Biotech, Cat# JX201-01) restriction sites, generating the recombinant transfer vector pFastBacHTB-Cap. This construct was subsequently transformed into DH10Bac competent cells (Thermo Fisher Scientific Inc., Cat# EC0113) for blue-white screening. The identified recombinant bacmid was transfected into Sf9 cells to generate recombinant baculovirus rBacHTB-Cap. Protein expression was analyzed by sodium dodecyl sulfate-polyacrylamide gel electrophoresis (SDS-PAGE) and Western blot using a Cap-specific monoclonal antibody (GeneTex, Cat# GTX634210). The self-assembly of Cap protein into virus-like particles (VLPs) was further verified by TEM.

2.3. Synthesis of Cap@ZIF-8-CpG vaccine

First, 2-methylimidazole (11.08 mg, 0.14 mmol) was added into 0.45 mL of H_2O, followed by sonication until fully dissolved. A Cap protein solution (0.45 mL, 500 μg/mL) was added into the above-mentioned solution, followed by stirring for 30 min at 25 °C. Then, 0.1 mL of a $Zn(NO_3)_2{\cdot}6H_2O$ (6.00 mg, 0.02 mmol) aqueous solution was

added into the reaction mixture, followed by stirring for 12 h at room temperature. The precipitate product was collected via centrifugation, washed thrice using phosphate-buffered saline (PBS), and vacuum dried at 25 °C for 24 h, yielding 4.1 mg of Cap@ZIF-8 white powder.

The Cap@ZIF-8 (5 mg) obtained was redispersed in CpG ODN solutions (2 mL, 100 nM) at room temperature. After stirring for 12 h, the precipitate was collected, washed thrice using PBS, and dried at 25 °C for 24 h. The product obtained was noted as the Cap@ZIF-8-CpG vaccine.

2.4. Preparation method of FITC-Cap

FITC (fluorescein isothiocyanate) was purchased from MedChemExpress. This reagent is primarily used to label Cap protein and to observe its uptake and distribution within cells [45,46]. Cap protein (10 mg) was dissolved in sodium carbonate buffer (10 mL, pH = 9.8, 25 × 10^{-3} M). Subsequently, FITC (200 μL, 1 mg mL^{-1}) was added into the solution and stir in the dark at 4 °C overnight to ensure complete reaction. After the reaction is complete, the entire mixture was transferred into a dialysis bag (MW 3 kDa) and dialyzed for 3 days to remove unbound FITC and other impurities. Finally, the purified mixture was dried in a freeze-dryer to obtain FITC-Cap, and the obtained FITC-Cap was stored at −20 °C for subsequent use.

2.5. Preparation of FITC-Cap@ZIF-8-CpG

Briefly, 10 mg of Cap@ZIF-8-CpG was dispersed in PBS (10 mL). Then, 0.2 mg of fluorescein isothiocyanate (FITC) was added into the mixture, followed by stirring for 12 h at 25 °C. FITC-Cap@ZIF-8-CpG was obtained via centrifugation and then washed thrice using PBS.

2.6. Loading capacity of Cap@ZIF-8-CpG

Encapsulation ability of Cap@ZIF-8-CpG for the Cap protein: The encapsulation capacity of the Cap protein was measured using the BCA protein quantitation kit as per the calibration curve of protein concentration and absorbance. After centrifugation of Cap@ZIF-8, the Cap protein concentration in the supernatant was detected using the BCA method. Each group was replicated thrice to eliminate experimental errors.

Adsorption capacity of Cap@ZIF-8-CpG for CpG: The supernatant was detected via UV–vis spectrophotometry at 256 nm. The adsorption quantity of CpG in Cap@ZIF-8-CpG was calculated and analyzed based on the standard curve.

2.7. Release experiments of Cap and CpG

An examination was conducted to study the sustained release of the Cap protein in Cap@ZIF-8-CpG under neutral and lysosomal environmental conditions: Cap@ZIF-8-CpG (20 mg, containing 1.02 mg Cap and 37.95 μg CpG) was immersed in 100 mL of a buffer solution (pH = 6.0 or pH = 7.4) at 37 °C. At a predetermined time interval, 2.0 mL of the solution was extracted and replaced with an equal volume of a fresh buffer solution under slight stirring conditions. This process was repeated and detected using the BCA method until the concentration of the Cap protein in the extract became constant. For the studying the release of CpG from Cap@ZIF-8-CpG, the operation was similar to the abovementioned experiments, except that the final level of CpG was detected via UV–vis spectrophotometry at 256 nm.

2.8. The protective effect of Cap@ZIF-8-CpG for CpG

Referring to the previous report, we've made minor adjustments [47]. CpG (12.5 μM) and Cap@ZIF-8-CpG suspension (containing 12.5 μM CpG) were each mixed with 25 μL of DNase I (HY-108882, MedChemExpress, 1.0 U/mL) and incubated at 37 °C for 30 min, respectively. After incubation, the samples were heated at 65 °C for 10 min to inactivate DNase I. For the Cap@ZIF-8-CpG group, the samples were centrifuged to remove the supernatant, and 25 μL of buffer solution (pH 5.0–6.0) was added to the tube to dissolve the ZIF-8 shell. Untreated CpG (12.5 μM) was used as the negative control. The integrity of CpG in three groups was analyzed by Agarose Gel Electrophoresis, using DNA marker DL 1000 (3591Q; purchased from Takara Biomedical Technology (Beijing) Co., Ltd.) as the molecular weight standard.

2.9. Thermal protective effect of Cap@ZIF-8-CpG

Based on the previous reference [48], Cap@ZIF-8-CpG and Cap protein samples (1 mL, containing equivalent 50 μg of Cap protein) were subjected to various temperature conditions (4, 25, 40, and 60 °C) for 3 h to investigate the thermal protective effect of the ZIF-8 shell on Cap protein. Cap protein and Cap@ZIF-8-CpG samples treated at 0 °C were defined as controls. Following treatment, the Cap@ZIF-8-CpG samples were washed with buffer solution (pH 5.0–6.0) to remove the encapsulation, and the protein in the supernatant was collected by centrifugation. The protein concentration in the supernatant of all experimental groups was measured using the BCA assay, and the activity of Cap protein was assessed by ELISA.

2.10. Cytotoxicity

PK-15 and RAW264.7 cells were selected to assess cytotoxic effects of ZIF-8, Cap@ZIF-8, and Cap@ZIF-8-CpG; each group included six parallel samples to minimize experimental errors. Briefly, ZIF-8, Cap@ZIF-8, and Cap@ZIF-8-CpG were diluted to concentrations of 3.125, 6.25, 12.5, 25.0, and 50.0 μg/mL with 2 % DMEM. Furthermore, cells were seeded into 96-well culture plates (~5000 cells per well) and incubated for 24 h in a5 % CO_2 environment at 37 °C. After washing thrice with PBS buffer, we sterilized 100 μL of each of ZIF-8, Cap@ZIF-8, and Cap@ZIF-8-CpG at different concentrations and added to each well followed by incubation for another 24 h, with untreated cells regarded as the blank control. Subsequently, 10 μL of the Cell Counting Kit-8 (CCK-8 kit, ABclonal Technology, RM02823) solution was added into each well, followed by further incubation for 4 h. The cell viability in each group was expressed as the percentage relative to the viable cells of the control group.

2.11. Cellular uptake efficiency

RAW264.7 cells were seeded into the cell culture dishes and incubated for 24 h. This was followed by further incubation with FITC-Cap or FITC-Cap@ZIF-8-CpG at 37 °C for 4 h. Residual substances were removed by means of washing with PBS several times, and the efficiency of cell uptake was analyzed via flow cytometry.

2.12. Endocytosis Inhibition

RAW 264.7 cells were plated in 6-well plates and incubated for 24 h. Subsequently, the cells were pre-incubated with various concentrations of inhibitors for 1 h: 50 μg/mL Methyl-β-cyclodextrin (MedChemExpress, HY-101461), 25 μg/mL Amiloride (MedChemExpress, HY-B0285), and 10 μg/mL Chlorpromazine (MedChemExpress, HY-12708). Then, the cells were washed with PBS and incubated with FITC-Cap@ZIF-8-CpG (100 μg/mL) for 6 h. Post-incubation, the cells were washed again with PBS and analyzed using a flow cytometer.

2.13. Cytokine assays in vitro

RAW264.7 and PK-15 cells were incubated with Cap@ZIF-8-CpG. RNA of the cells was obtained using RNA-easy Isolation Reagent (Vazyme#R701), and the concentration was determined using the Nanodrop 2000 system (Thermo Fisher Scientific Inc.). Subsequently, the RNA

extracted was reverse transcribed into cDNA (Vazyme#R323). DNA quantification was performed using qPCR special premix (Vazyme#R711). Secretions of tumor necrosis factor alpha (TNF-α) and IL-6 in RAW264.7 and PK-15 cells from different groups were assessed via quantitative reverse transcription polymerase chain reaction (qRT-PCR) analysis. Gene expression levels were calculated using the $2^{-\Delta\Delta ct}$ method, and all PCR reactions were conducted in triplicate.

2.14. Hemocytolysis

Mice blood was collected, following which red blood cells (RBCs) were isolated (2000 rpm, 10 min). Subsequently, the RBCs were washed five times using Dulbecco's PBS (D-PBS, Beijing Solarbio, Cat#D1040) and then diluted 10-fold using D-PBS. Meanwhile, Cap@ZIF-8-CpG solutions with the following concentrations were prepared: 0, 12.5, 25, 50, 100, 150, 200, 400, and 800 μg/mL, which contains Cap (0, 0.64, 1.27, 2.55, 5.10, 7.65, 10.20, 20.41, and 40.82 μg/mL) and CpG (0, 24, 47, 95, 190, 285, 380, 760, and 1520 ng/mL). Thereafter, fresh diluted mice blood was added into the abovementioned 10 Cap@ZIF-8-CpG solutions with different concentrations, followed by incubation at 37 °C for 4 h; centrifugation resulted in stratification. The supernatant (100 μL per well) was transferred into a 96-well plate, and the optical density (OD) value was measured at 570 nm using a microplate reader (three parallel experiments per group). The hemolysis rate of Cap@ZIF-8-CpG was calculated as follows:

$$\text{Hemolysis ratio (\%)} = (OD_{samples} - OD_{NC})/(OD_{PC} - OD_{NC}) \times 100,$$

where $OD_{samples}$, OD_{PC} (OD positive), OD_{NC} (OD negative) are the absorbance values of the samples, DI water, and D-PBS, respectively.

2.15. In vivo biosafety of Cap@ZIF-8-CpG

The *in vivo* biosafety of Cap@ZIF-8-CpG was systematically studied utilizing mice as model animals to evaluate its potential application as a nanovaccine (No. IASVM-2023-004). Female BALB/c mice were randomly divided into six groups (n = 5) and then subcutaneously injected with 100 μL of PBS, Cap (0.5 mg/mL), Cap + CpG (0.5 mg/mL, 350 nM), Cap + ZIF-8 + CpG (0.5 mg/mL, 9.3 mg/mL, 350 nM), Cap@ZIF-8 (9.8 mg/mL), and Cap@ZIF-8-CpG nanovaccine (9.8 mg/mL), respectively. *Blood routine test:* Thereafter, blood samples of the immunized mice across the six groups were collected from the retro-orbital plexus on day 7, and various blood indicators were meticulously measured using an auto hematology analyzer (Mindray Animal Care BC-30 Vet). *Analysis of tissue inflammation at the injection site:* Injection site tissues of the mice were shaved and removed on days 0 and 7 after subcutaneous injection. The tissues were fixed using 4 % paraformaldehyde, fixed, sliced, and then, stained with hematoxylin and eosin (H&E) for local inflammation study via microscope photography.

2.16. Animal experiment

Female BALB/c mice (~5-week old) were obtained from Jinan Pengyue Experimental Animal Breeding Co., Ltd. The entire animal experimental protocol strictly adhered to the guidelines established by "Guidance for the Care and Use of Laboratory Animals" and were approved by the Experimental Animal Ethics Committee of Shandong Academy of Agricultural Sciences, Institute of Animal Sciences and Veterinary Medicine (No. IASVM-2023-004).

The mice were randomly divided into six groups (10 mice in each group), with each mice receiving 100 μL of any one of the following agents via subcutaneous injection: PBS, Cap (0.5 mg/mL), Cap + CpG (0.5 mg/mL, 350 nM), Cap + ZIF-8 + CpG (0.5 mg/mL, 9.3 mg/mL, 350 nM), Cap@ZIF-8 (9.8 mg/mL), and Cap@ZIF-8-CpG nanovaccine (9.8 mg/mL, the Cap and CpG contents are 50 μg and 1.86 ng in the formulation, respectively). Except for the PBS group, each group was administered equivalent doses of the Cap protein (50 μg). Followed by a 14-day observation period (i.e., at the 14th day post the first vaccination), the second immunization was administrated using the same doses of the agents. The growth curve of mouse weight with time under various conditions was recorded.

2.17. Analysis of related antibodies and cytokines

Analysis of IgG, IgG1, and IgG2a: PCV2-specific IgG, IgG1, and IgG2a expressions were determined via ELISA. Briefly, the blood samples of the immunized mice were collected at 14th and 28th day postinoculation (dpi). Prior to analysis, the serum samples were subsequently separated and diluted 100 times using the sample diluent. Following this, 100 μL of each diluted sample was introduced into the 96-well microtiter plates coated with the PCV2 antigen, and the coated plates were blocked and incubated for 30 min at 25 °C ± 3 °C. The coating solution in each well was discarded, and the plates were washed several times with the washing solution provided to eliminate any unreacted antibodies. Subsequently, 100 μL of HRP-labeled goat antimouse IgG (H + L) (1:250 in PBS), IgG1 (1:5000 in PBS), and IgG2a (1:5000 in PBS) were dispensed into plates and incubated for another 30 min at 25 °C ± 3 °C. Thereafter, the plates were washed thrice, 100 μL of a 3,3′,5,5′-tetramethylbenzidine chromogen solution was added, and the plates were placed in the dark for 15 min at 25 °C. Finally, after adding 50 μL of a stop buffer, the absorbance was immediately detected at 450 nm using a microplate reader (BioTeK Instruments, Inc., ELX808).

Cytokine Assay: Blood samples were collected at 21st dpi, and sera were obtained via centrifugation. Levels of IFN-γ, IL-4, and IL-2 were detected using ELISA kits (Meimian, MM-0182M1, MM-0165M1, and MM-0701M1).

2.18. Evaluation of the immune activation

To assess the activation of the immune response, spleen cells were isolated from immunized mice across various experimental groups at the 21st day and adjusted to a suitable cell concentration using a PBS buffer. Thereafter, the spleen cells were stained using the APC antimouse CD3 (BioLegend, 100236), FITC antimouse CD4 (BioLegend, 100405), and PE antimouse CD8a antibodies (BioLegend, 100707) and employed to meticulously analyze T-cell subsets via flow cytometry.

2.19. Challenge test

Thirty female BALB/c mice were randomly assigned to six groups (n = 10) to assess the protective immunity of the Cap@ZIF-8-CpG nanovaccine: PBS, Cap, Cap + CpG, Cap + ZIF-8 + CpG, Cap@ZIF-8, and Cap@ZIF-8-CpG; each group received two subcutaneous injections with 100 μL of various agents. Subsequently, the mice were challenged with PCV2 (100 μL, 50 % tissue culture infectious dose = 10^6) via intraperitoneal injection at 28th day, and we recorded the growth curve of mouse weight with time under various conditions. The mice were euthanized via cervical dislocation at 14th, 21st, and 28th days after PCV2 inoculation, after which specimens of heart, liver, spleen, lung, and kidney were collected. PCV2 viral DNA was extracted from the specimens using a FastPure viral DNA/RNA mini kit (Vazyme #RC311), and a real-time fluorescence PCR kit was used for the detection of PCV2 (Hunan Guanmu Biotechnology Co., Ltd, GM11005)

2.20. H&E and immunohistochemical analysis

On the 14th day after infection, liver, spleen, and lung tissue samples were collected from mice across the six groups, fixed in 10 % formalin, dehydrated, paraffin-embedded, sliced into 5 μm–thick tissues, and stained using H&E. To visually and clearly comprehend the distribution of PCV2 in spleen and lung, the sections were incubated with the PCV2 Capsid antibody (Gene Tex. Inc., GTX634210), and the nucleus was

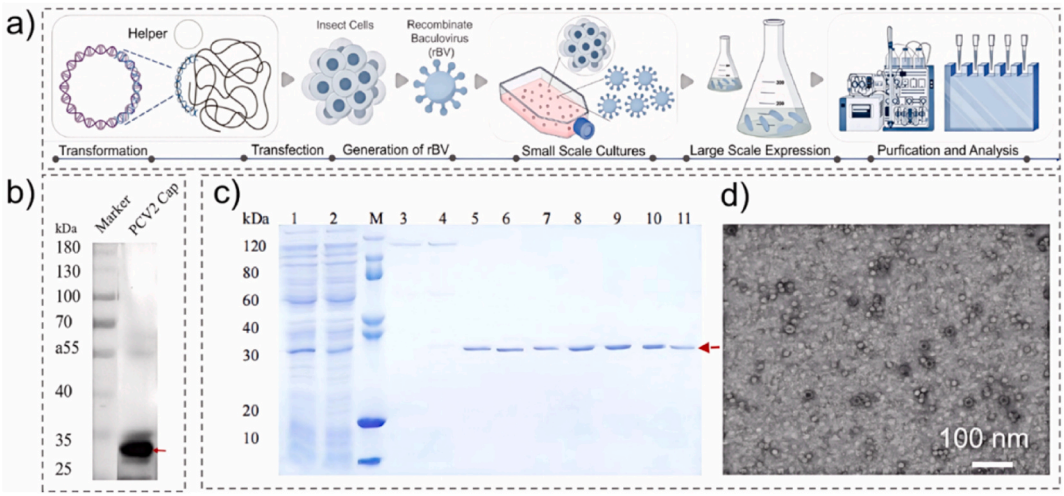

Fig. 1. (a) Process diagram of expression and identification of the Cap protein. (b, c) Western blot and sodium dodecyl sulfate–polyacrylamide gel electrophoresis (SDS–PAGE) analysis. (d) Transmission electron microscopy (TEM) images of the porcine circovirus type 2 (PCV2) Cap protein.

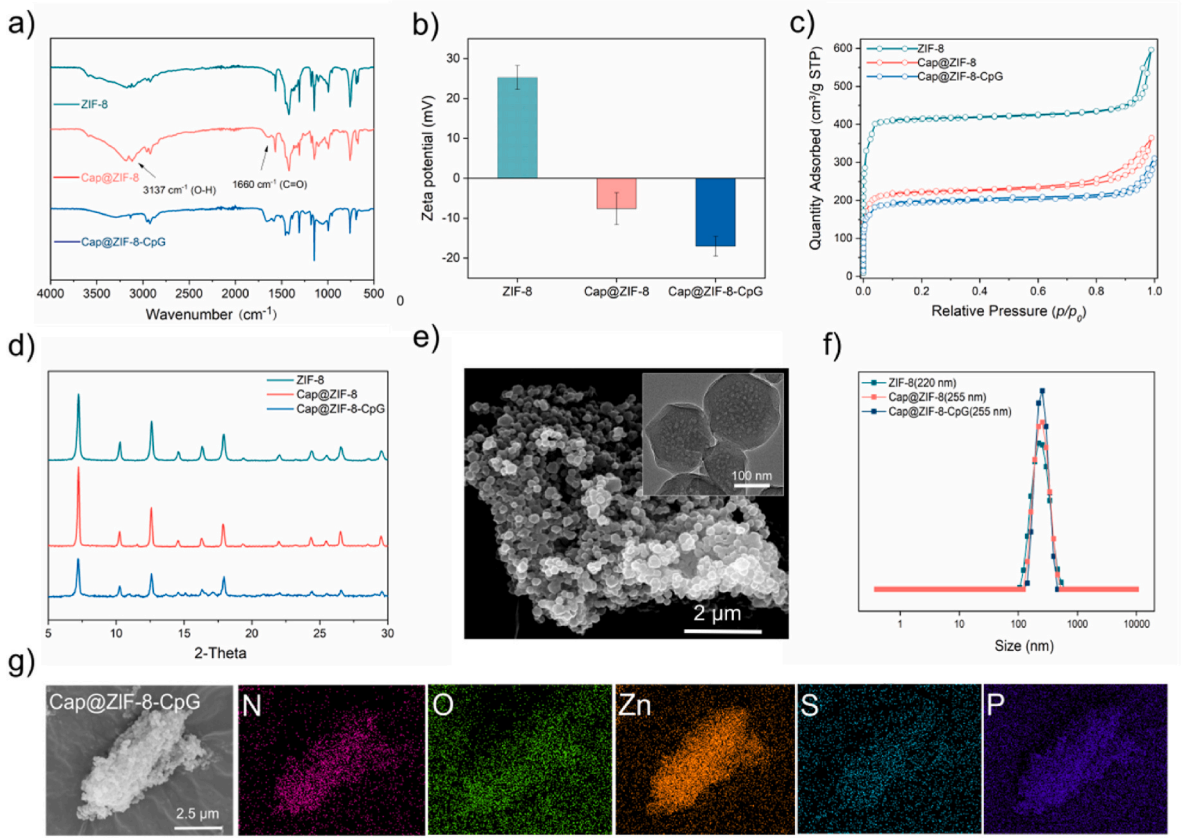

Fig. 2. (a) Fourier-transform infrared spectroscopy (FT-IR) spectra. (b) Zeta potentials. (c) N_2 adsorption/desorption isotherms. (d) Powder X-ray diffraction (PXRD) patterns. (e) Scanning electron microscopy (SEM) images of Cap@ZIF-8-CpG, inset: transmission electron microscopy (TEM) images. (f) Hydrated particle size distribution. (g) Energy-dispersive spectroscopy mapping images of Cap@ZIF-8-CpG and relevant images of the elements N, O, Zn, S, and P.

marked using 4′,6-diamidino-2-phenylindole (DAPI, Solarbio Cat#C0065). All histopathological alterations and pathological damage were recorded and evaluated using a metallographic microscope (BX51, Olympus)

2.21. Statistical analysis

The statistical calculation and analysis were performed using the Origin 8.0 software. All data presented herein were expressed as mean ± standard deviation. One-way analysis of variance was followed by a Tukey's multiple comparisons test. The considerable difference was represented using asterisks ($*P < 0.05$, $**P < 0.01$, and $***P < 0.001$).

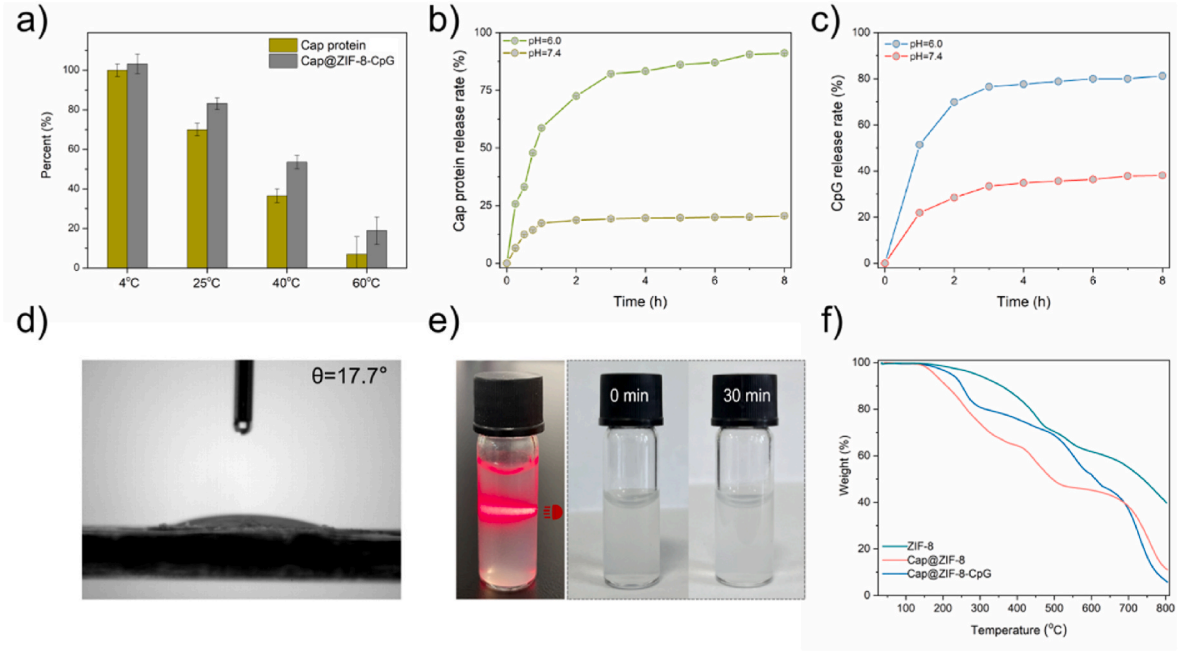

Fig. 3. (a) Thermostability of Cap was assessed by detecting the reactogenicity at various temperatures for 3h. (b, c) pH-responsive release of Cap@ZIF-8-CpG was assessed at pH = 7.4 and 6.0. (d) Water contact angles of Cap@ZIF-8-CpG. (e) Dispersibility of Cap@ZIF-8-CpG (5.0 mg/mL) in PBS. (f) Thermogravimetric analysis traces of ZIF-8, Cap@ZIF-8, and Cap@ZIF-8-CpG.

3. Results and discussion

3.1. Expression and identification of the Cap protein

As shown in Fig. 1a, the PCV2 ORF2 gene sequence was optimized and synthesized using the baculovirus expression system, successfully harvested rBacHTB-Cap. The Cap protein was then purified and analyzed via SDS–PAGE and Western blot. Results demonstrated abundant expression of the PCV2 Cap protein, with a clear specific band at 30 kDa (Fig. 1b and c). Moreover, further observation via TEM revealed that the recombinant Cap protein exhibited uniform, nonfixed morphology particles with a diameter of ~10–20 nm (Fig. 1d). All the abovementioned results indicated that the Cap protein expressed by the baculovirus expression system could form VLPs and had exhibited reactivity, which provided important materials for further exploring the novel PCV2 vaccine.

3.2. Characterization of Cap@ZIF-8-CpG

Herein, the Cap protein was successfully encapsulated within ZIF-8 to obtain Cap@ZIF-8 in situ. Subsequently, CpG was adsorbed onto Cap@ZIF-8, obtaining Cap@ZIF-8-CpG. For comparison, ZIF-8 was synthesized as per the existing literature. As shown in Fig. 2a, FT-IR spectra distinctly revealed the characteristic stretching vibrations of the C=O bond (1660 cm^{-1}) and O–H bond (3137 cm^{-1}), originating from the Cap protein. Meanwhile, an absorbance peak (262 nm) attributed to Cap was observed in the UV–vis spectrum of the nanoparticles synthesized (Fig. S1). In addition, TEM elemental mappings indicated uniform distribution of the elements C, N, O, Zn, and S in Cap@ZIF-8 (Fig. S2), which evidenced the successful encapsulation of the Cap protein in Cap@ZIF-8. The zeta potential analysis also evidenced the successful synthesis of Cap@ZIF-8-CpG. The zeta potential of Cap@ZIF-8-CpG decreased from 25.2 (ZIF-8) to −17.0 mV because of the negative charge of Cap and CpG, as shown in Fig. 2b. The N_2 adsorption characteristics of Cap@ZIF-8-CpG were assessed at 77 K to evaluate its permanent porosity (Fig. 2c). The N_2 adsorption capacity and Brunauer–Emmett–Teller (BET) surface area of Cap@ZIF-8-CpG were measured to be 309.9 cm^3/g and 792.8 m^2/g, respectively. The average pore size distribution was observed to be centered at ~1.09 nm, as determined via the Barrett–Joyner–Halenda analysis (Fig. S3). In contrast with the BET results of Cap@ZIF-8-CpG, those of ZIF-8 and Cap@ZIF-8 exhibited greater pore sizes, higher N_2 adsorption capacities, and larger specific surface areas. This was attributed to the encapsulation of the Cap protein and the loading of CpG, which occupied a considerable portion of the pore volume within ZIF-8. Moreover, the X-ray diffraction patterns shown in Fig. 2d exhibited no considerable variations between Cap@ZIF-8-CpG, Cap@ZIF-8, and ZIF-8, indicating that the crystallization of obtained Cap@ZIF-8-CpG was highly retained. The morphology and size of Cap@ZIF-8-CpG were analyzed via SEM and TEM (Fig. 2e). The images indicated that the average size of Cap@ZIF-8-CpG particles was ~200 nm, resembling those of ZIF-8 and Cap@ZIF-8, as further confirmed via DLS analysis (Fig. 2f). Meanwhile, the energy-dispersive spectroscopy mapping images revealed uniform distribution of the elements N, Zn, O, S, and P in Cap@ZIF-8-CpG nanoparticles, further confirming the presence of Cap and CpG in the nanoparticles (Fig. 2g).

Test results of the BCA assay kit revealed that ZIF-8 exhibited a remarkable encapsulation efficiency of 93 % for Cap at a Cap concentration of 500 μg/mL (Fig. S4). Moreover, Cap@ZIF-8 still maintained remarkable adsorbent properties. The obtained Cap@ZIF-8 with a CpG ODNs solution (100 nM) at 25 °C for 12 h, CpG-loaded Cap@ZIF-8-CpG was efficiently generated. The loading amount of CpG ODNs was calculated to be 0.18 nmol as per the standard curve of the UV–vis spectrum (Fig. S5). It underscored the immense potential of ZIF-8 in loading antigens and enhancers owing to its abundant cavities, thus validating the suitability of Cap@ZIF-8-CpG as a robust vaccine delivery system.

3.3. Protein release and stability performance of Cap@ZIF-8-CpG

Notably, the encapsulation of the Cap protein considerably enhances its resistance to denaturation [49]. Consequently, Cap@ZIF-8-CpG and naked Cap were incubated at various temperatures for 3 h, and the reactogenicity was revealed via ELISA analysis. As shown in Fig. 3a, the

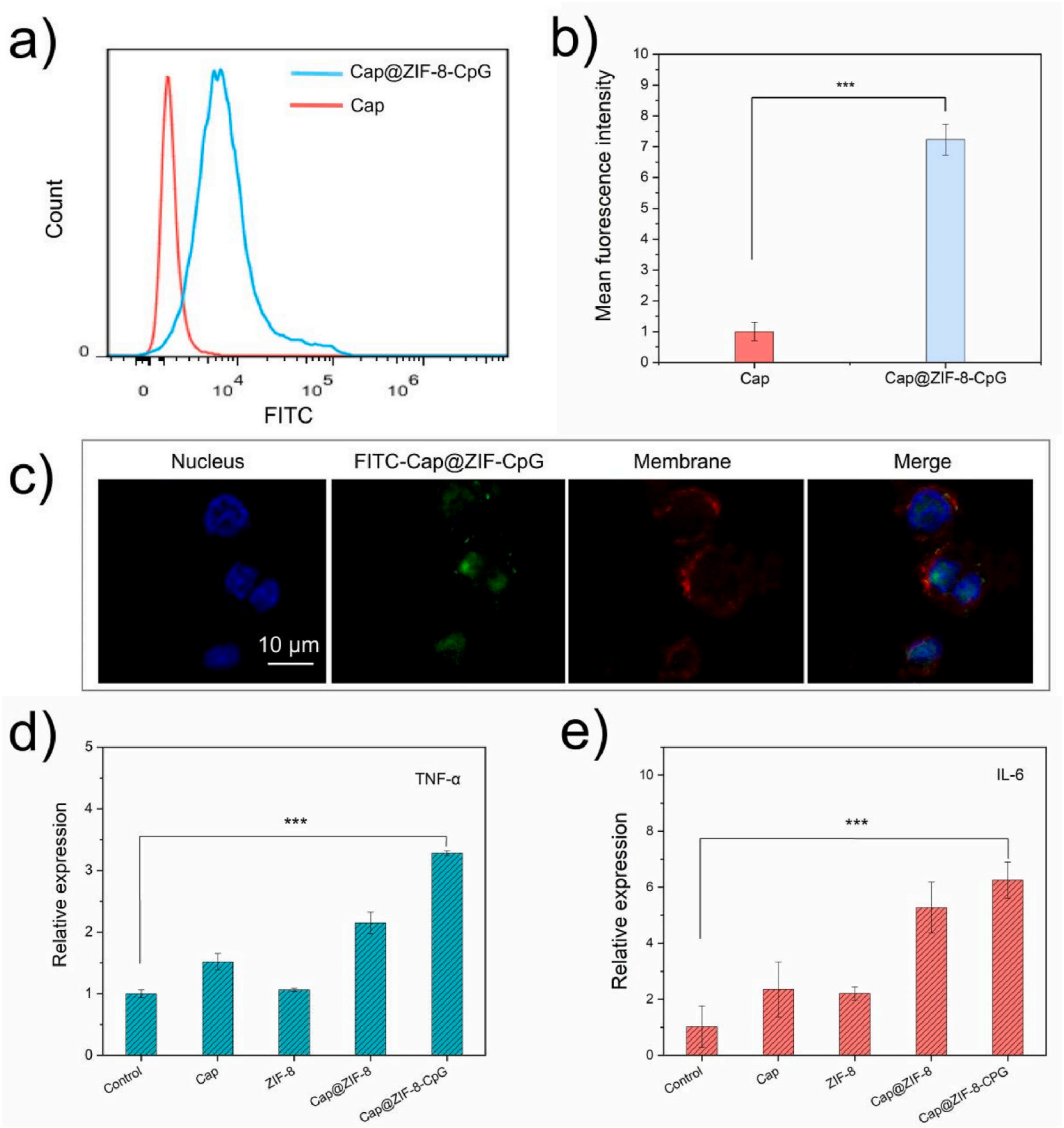

Fig. 4. (a, b) Cellular uptake efficiency for Cap@ZIF-8-CpG was evaluated by flow cytometry analysis. (c) Fluorescence images of cells treated with FITC-Cap@ZIF-8-CpG for 4 h. (d) Tumor necrosis factor alpha (TNF-α) and (e) interleukin-6 (IL-6) secretion analysis of cellular inflammatory factors stimulated by Cap@ZIF-8-CpG.

activity percentage of naked Cap gradually decreased with escalating temperatures, whereas Cap@ZIF-8-CpG delivered better performance. By contrast, the activity retention of Cap@ZIF-8-CpG was considerably higher than that of naked Cap by three times at 60 °C. These findings underscored the effectiveness of biomineralization of ZIF-8 in bolstering the thermal stability and activity of proteins, presenting a valuable approach to tackling challenges associated with cold chain transportation of vaccines. Meanwhile, we treated Cap@ZIP-8-CpG with DNase, further confirming that ZIF-8 also has an excellent protective effect on CpG after adsorption (Fig. S6). Furthermore, Cap@ZIF-8-CpG exhibited pH-sensitive release of the antigen and CpG, a crucial feature enabling nanovaccines to stimulate an immune response effectively. As shown in Fig. 3b and c, the pH-responsive release performance of Cap@ZIF-8-CpG was examined in PBS (pH = 7.4) and another buffer (pH = 6.0) at 37 °C. Results demonstrated that Cap@ZIF-8-CpG exhibited a rapid release of Cap and CpG, reaching 82.1 % and 76.5 %, respectively, after 3 h at pH = 6.0. Subsequently, the release rate slowed down, eventually becoming >90 % and >80 % after 7 h of incubation. Nevertheless, in a PBS buffer (pH = 7.4), only ~17.3 % and ~35.6 % of Cap and CpG released after 8 h, respectively. Dispersion of nanovaccines is a crucial factor in vaccine development. Water contact angles of Cap@ZIF-8-CpG were measured to be 17.7° ± 2°, indicating that this material possessed hydrophilic properties (Fig. 3d). Subsequently, the widely utilized PBS was selected as the dispersion medium to assess the dispersion of Cap@ZIF-8-CpG. Upon dispersing Cap@ZIF-8-CpG in PBS, the solution showed a pronounced Tyndall effect and maintained remarkable stability for 30 min (Fig. 3e), demonstrating that Cap@ZIF-8-CpG was minorly influenced by van der Waals forces and hydrogen bonding and further implying that the Cap@ZIF-8-CpG nanovaccine synthesized would not compromise its injectability. Furthermore, TGA revealed that Cap@ZIF-8-CpG maintained thermal stability at up to 130 °C, demonstrating its remarkable thermal stability. In comparison with ZIF-8, Cap@ZIF-8-CpG exhibited a more obvious weight loss, attributed to the degradation of Cap and CpG (Fig. 3f).

3.4. Cellular uptake and immune activation of Cap@ZIF-8-CpG

Internalization efficiency of macrophages for the vaccine significantly affected the activity of the immune process. Consequently, we employed green fluorescence FITC to label Cap@ZIF-8-CpG, fabricating FITC-Cap@ZIF-8-CpG complexes to investigate Cap@ZIF-8-CpG's

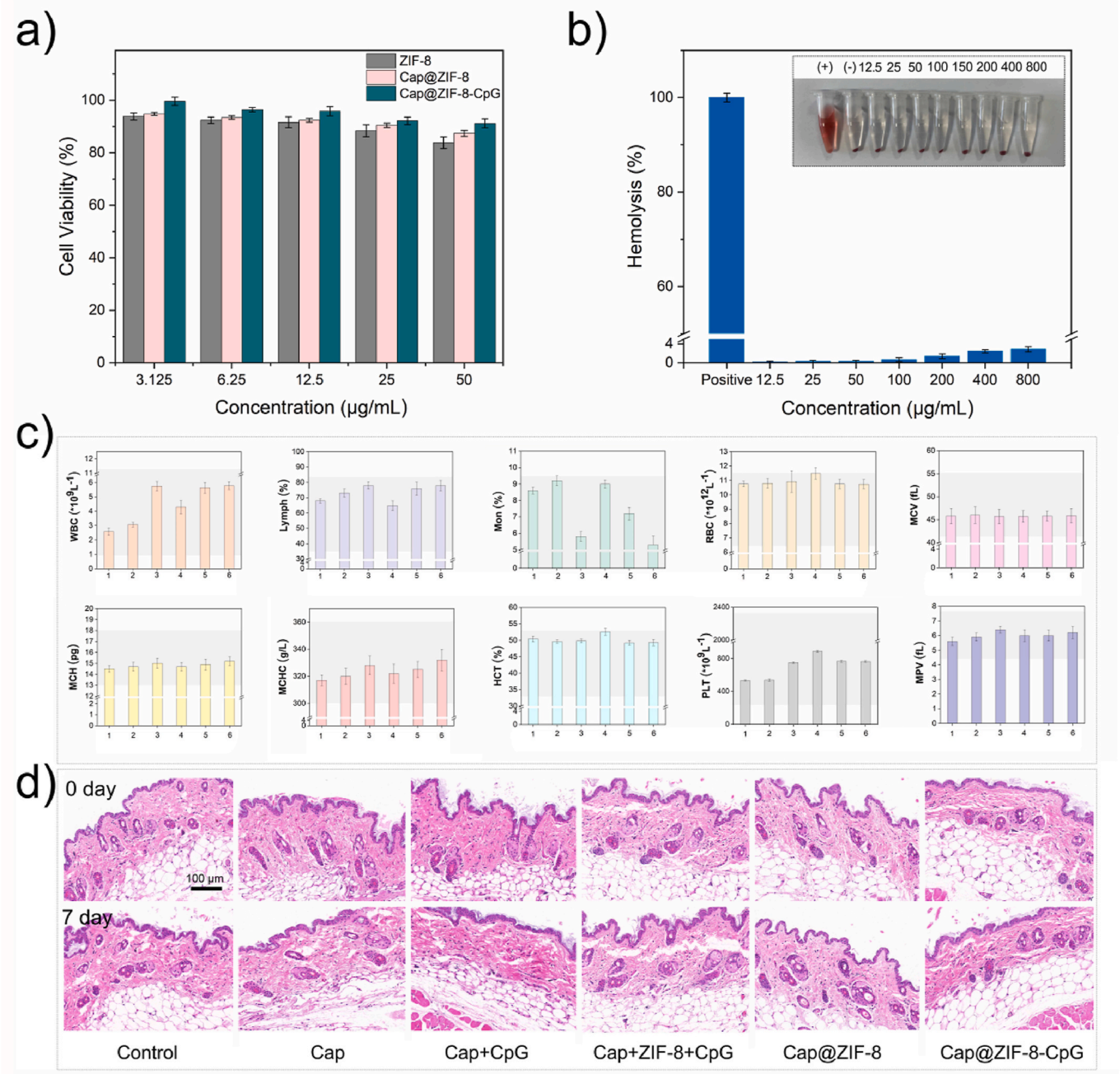

Fig. 5. (a) Cell viability of RAW 264.7 cells treated with ZIF-8, Cap@ZIF-8, and Cap@ZIF-8-CpG at different concentrations. (b) Hemolysis assays of Cap@ZIF-8-CpG at 0–800 μg/mL. (c) Blood analysis for the first vaccinated mice on 7th dpi (1: Control, 2: Cap, 3: Cap + CpG, 4: Cap + ZIF-8 + CpG, 5: Cap@ZIF-8, and 6: Cap@ZIF-8-CpG; the gray area indicates the normal range for each parameter). (d) H&E inflammation analysis of the injection site for the first vaccinated mice on 0th or 7th dpi.

cellular uptake efficiency. Meanwhile, RAW264.7 cells was selected in our cellular research. It is attributed to the fact that, as a type of macrophage cell line, RAW264.7 cells are extensively employed in the study of various mechanisms associated with immune responses and inflammation. Flow cytometry analysis substantiated the efficient cellular uptake of Cap@ZIF-8-CpG (Fig. 4a and b), indicating augmentation in Cap@ZIF-8-CpG-mediated active-delivery, which may bolster immune response and vaccination efficacy. Moreover, CLSM further validated the dramatic Cap@ZIF-8-CpG uptake efficiency of RAW264.7 cells (Fig. 4c). It has been reported that the primary pathways for nanoparticles to enter cells include macropinocytosis, caveolin-mediated endocytosis, and clathrin-mediated endocytosis [50]. Among them, amiloride can inhibit macropinocytosis, methyl-β-cyclodextrin can inhibit caveolin-mediated endocytosis, and chlorpromazine can inhibit clathrin-mediated endocytosis. The experimental results revealed that the cellular uptake efficiency of Cap@ZIF-8-CpG was significantly affected after the addition of chlorpromazine and amiloride. In contrast, treatment with methyl-β-cyclodextrin had no significant impact on the endocytosis of Cap@ZIF-8-CpG. In conclusion, it can been concluded that the internalization of Cap@ZIF-8-CpG into cells is not primarily dependent on caveolin-mediated endocytosis, but rather occurs mainly through clathrin-mediated endocytosis and macropinocytosis (Fig. S7). Free Cap protein entered cells via passive diffusion, resulting in suboptimal absorption efficiency. By contrast, Cap@ZIF-8-CpG was able to adeptly cross the cell membrane via clathrin-mediated endocytosis and macropinocytosis, thus exhibiting robust cellular internalization [51]. Clearly, the encapsulation of ZIF-8 effectively increased the shuttle of antigens into the cells. Moreover,

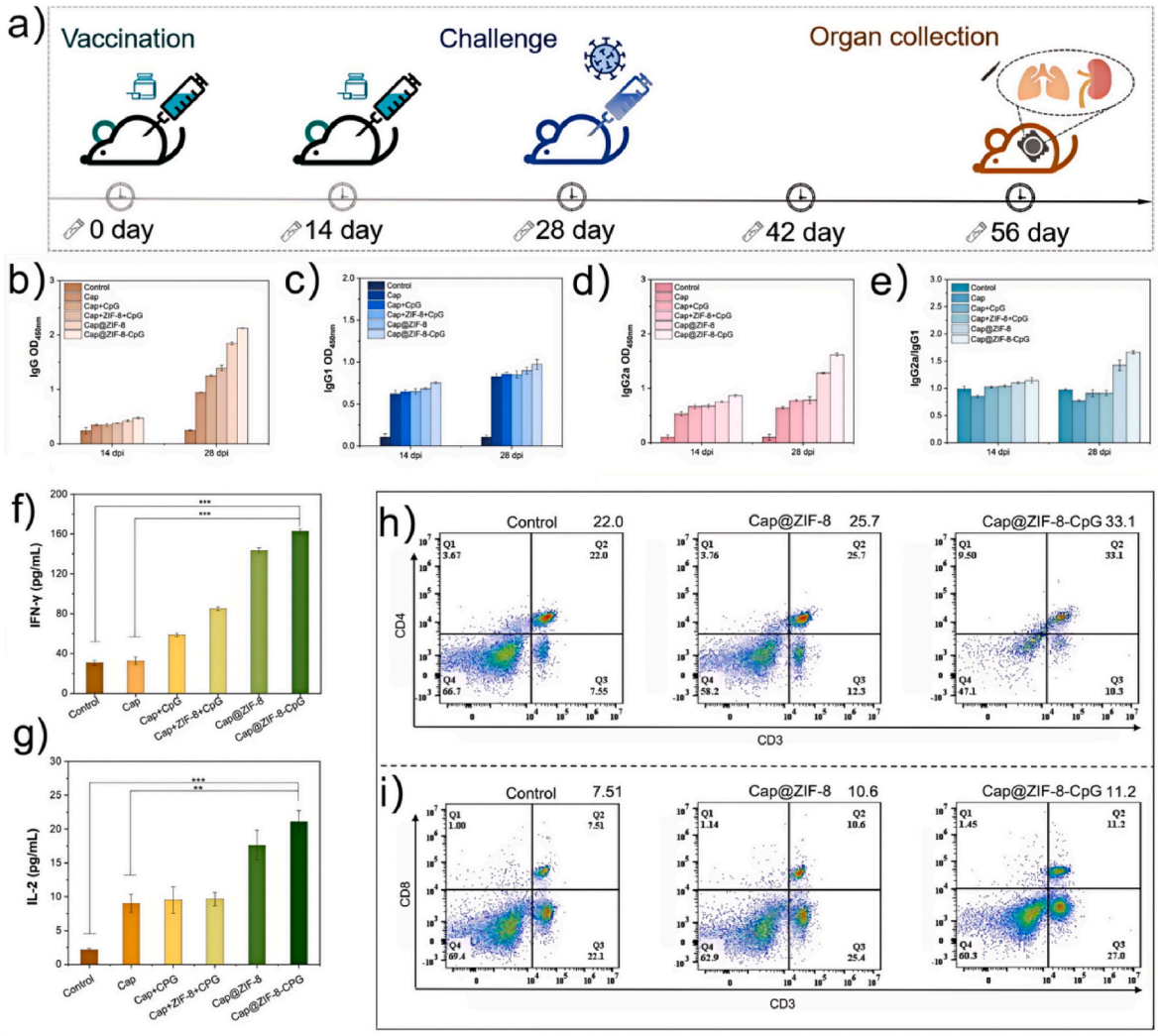

Fig. 6. (a) Scheme of the experimentation. (b–e) Levels of Cap-specific IgG, IgG1, IgG2a, and IgG2a/IgG1 at 14th and 28th dpi were quantified via ELISA. (f, g) Cytokine secretion of IFN-γ and IL-2 on 21 dpi from different immunized mice, (**$P < 0.01$, and ***$P < 0.001$ indicates a significant difference). (h, i) Flow cytometry analysis of $CD3^+CD4^+$ and $CD3^+CD8^+$ T cells on 21st dpi.

we investigated the immunostimulatory effect of Cap@ZIF-8-CpG. The secretion of immunostimulatory cytokines serves as a pivotal indicator of APC activation, fundamental to establishing an immune response effectively. After incubating RAW264.7 cells with various samples, the secretion levels of TNF-α and IL-6 were quantified via qRT-PCR analysis. As shown in Fig. 4d and e, the secretion of TNF-α and IL-6 stimulated by Cap@ZIF-8-CpG was nearly two to three fold greater than that induced by Cap or ZIF-8, indicating stronger immune responses, which suggested that Cap@ZIF-8-CpG possessed better immune stimulatory capabilities *in vitro*.

3.5. Biosafety of Cap@ZIF-8-CpG in vitro and in vivo

Undoubtedly, biosafety serves as the cornerstone for vaccine innovation; hence, we conducted a series of correlation assessments on the Cap@ZIF-8-CpG nanovaccine. As shown in Fig. 5a, even at a concentration of 50 μg/mL, the survival rates of RAW264.7 and PK-15 cells treated with Cap@ZIF-8-CpG exceeded 91.18 % and 89.58 % *in vitro*, respectively (Fig. S8), indicating the nanovaccine exhibited negligible cytotoxicity. Moreover, the results of hemolysis tests gave the biosafety argument of Cap@ZIF-8-CpG. No notable hemolysis was observed upon increasing the dose of Cap@ZIF-8-CpG to 800 μg/mL, revealing that the vaccine posed no injection-related risk (Fig. 5b). Following the administration of the Cap@ZIF-8-CpG nanovaccine, physiological responses and health conditions of the inoculated mice were meticulously observed. No notable changes were noted in the subjects across the different groups during the monitoring period. To assess the internal health of the mice at a cellular level, blood samples were taken at 7th dpi. Similar to that for the control group, the blood biochemical indicators of all experimental groups were within normal ranges (Fig. 5c), including RBC count, mean corpuscular hemoglobin, hematocrit, mean corpuscular hemoglobin concentration, white blood cell count, lymphocyte count, monocyte percentage, and platelet count. Furthermore, H&E staining of skin tissues at the injection sites revealed no damage at a dose of 500 μg/mL (the content of the Cap protein). Relative to before injection (0 day), no obvious pathological alterations, such as severe nodules and inflammation, were observed in the skin tissue at 7th dpi. (Fig. 5d).

3.6. Immune activity evaluations of Cap@ZIF-8-CpG

To verify the immune activity of Cap@ZIF-8-CpG, we further investigated its immune response to heterologous antigens in the mouse model. Mice were randomly divided into six groups and were inoculated with diverse samples via subcutaneous injection, including PBS, Cap, Cap + CpG combination, Cap + ZIF-8 + CpG combination, Cap@ZIF-8,

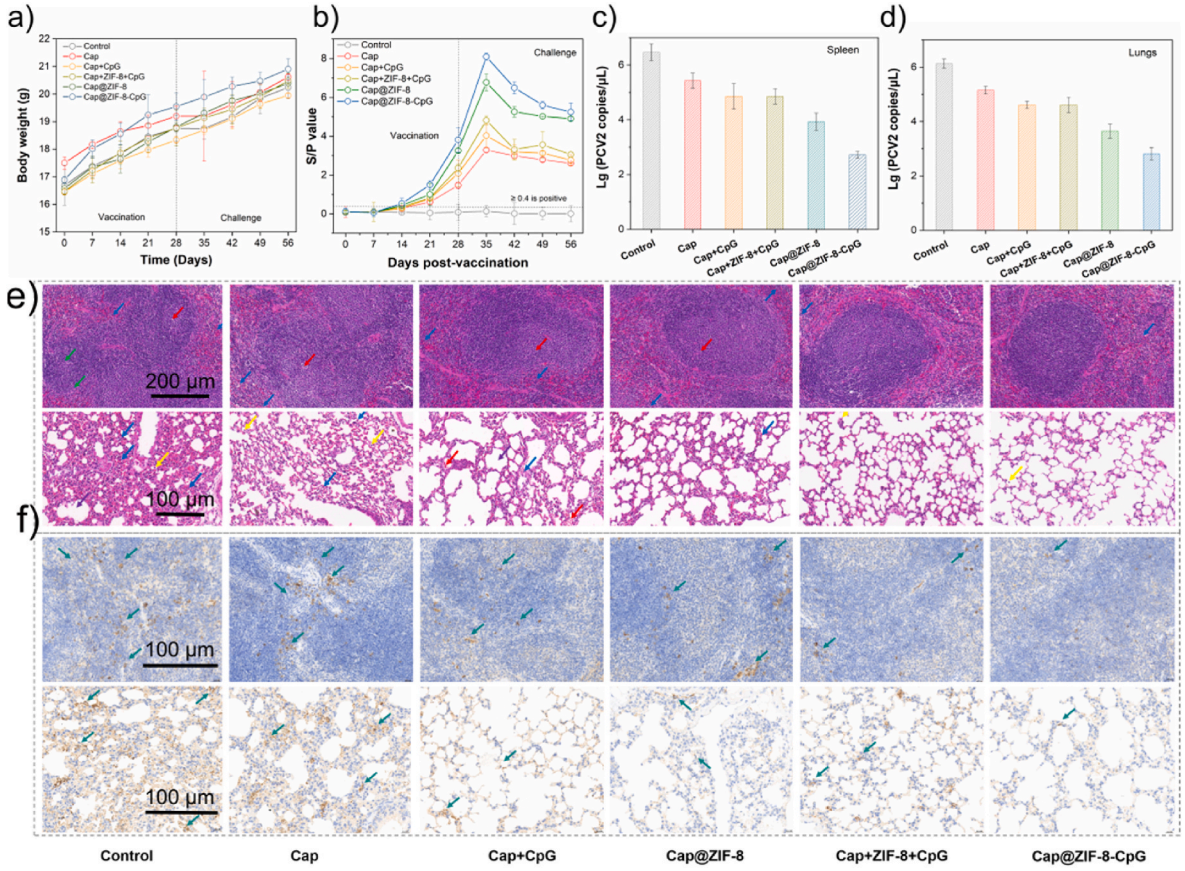

Fig. 7. (a) Weight changes and (b) specific antibody levels of various injection groups were consecutively observed for 56 days. (c, d) Virus amounts of spleen and lungs were detected in each group on 14th day post challenge. (e) H&E staining of spleen and lungs tissues in different groups, Spleen: White pulp with marginal zone (green arrow), Neutrophils (blue arrow), Lymphocyte necrosis in the white pulp (red arrow). Lung: Neutrophils (blue arrow), Widening of alveolar septa, Compensatory alveolar dilatation (purple arrow), Macrophages (yellow arrow), Alveolar hemorrhage (red arrow). (f) Immunohistochemical images of spleen and lungs tissues, Positive cells (cyan arrow).

and Cap@ZIF-8-CpG (Fig. 6a). Results unequivocally demonstrated that at 14th and 28th dpi, the levels of anti-Cap-IgG activated by the Cap@ZIF-8-CpG nanovaccine preceded those induced in the Cap, combination, and Cap@ZIF-8 groups, implying its ability to induce a robust humoral immune response (Fig. 6b). Relative to the combination group at 28th dpi, the anti-Cap-IgG secretion level in the Cap@ZIF-8-CpG group nearly doubled, which demonstrated that the porous architecture and hydrogen bonding interactions inherent in ZIF-8 played a pivotal role in regulating the sustained release of Cap antigens. Therefore, we hypothesized that the Cap@ZIF-8-CpG platform facilitated the codelivery of Cap and CpG into APCs and efficiently safeguarded them from degradation. This led to a synergy between Cap and CpG within the "antigen reservoir" created by the porous ZIF-8, whereby their interactions were enhanced [52]. Subsequently, we quantified the IgG1 and IgG2 levels and calculated the IgG2a/IgG1 ratios at 14th and 28th dpi (~1.1 and 1.6, respectively) (Fig. 6c–e). Understanding the Th1-type (cellular) and Th2-type (humoral) immune responses with respect their contribution to IgG activation revealed that Th1 cell–mediated immunity gradually played a predominant role as the immune cycle progressed. In addition, inflammatory cytokines are recognized for their critical role in modulating the proliferation and differentiation of various cell types, as well as exerting substantial regulatory effects on immune responses. On 21st dpi, the serum of mice was collected and the cytokine levels of IFN-γ, IL-2, and IL-4 were assayed via ELISA (Fig. 6f and g and Figs. S9–S12). In contrast with the Cap antigen administered alone, results indicated that both MOF-encapsulated vaccines elicited Th1-biased antibody responses. Clearly, the Cap@ZIF-8-CpG nanovaccine triggered the most pronounced secretion of IFN-γ, IL-2, and IL-4 compared with other groups. However, the Cap group only resulted in modest induction of IFN-γ secretion, with levels being ~30 % of the Cap@ZIF-8-CpG group's. These findings suggested that Cap@ZIF-8-CpG enhanced the cellular uptake of Cap and CpG, thereby boosting immunostimulatory activity. Meanwhile, the identification of total $CD8^+$ CTLs and $CD4^+$ T cells supported the aforementioned standpoint. Spleen cells from each group were harvested at 21st dpi and subsequently stained with anti-CD3-APC and either anti-CD4-FITC or anti-CD8a-PE antibodies for flow cytometric analysis. As evident from Fig. 6h and i and Fig. S13, Cap@ZIF-8-CpG exhibited superior efficacy in stimulating the proliferation of $CD8^+$ CTLs and $CD4^+$ T cells in comparison with the Cap group or any combination group. These collective outcomes highlighted the potential of Cap@ZIF-8-CpG in enabling the simultaneous delivery of Cap and CpG to APCs, thereby triggering potent humoral immune responses.

To evaluate the protective efficacy of the Cap@ZIF-8-CpG nanovaccine, mice in the six groups were subjected to a challenge with PCV2 virus at 28th dpi. Each mouse was administered 100 μL of a PCV2 virus solution via intraperitoneal injection, and their blood samples were systematically collected on days 7, 14, 21, and 28 postchallenge. On the 42nd day, a subset of mice was euthanized and their spleens and lungs were excised and partitioned into two sections. One section was processed for the detection of total RNA and DNA via qPCR, while the other section was preserved for histopathological analysis. During the experimental period, the health conditions of the mice were closely monitored. Remarkably, following the PCV2 challenge, the mice maintained normal feeding habits and water intake and displayed good mental states, coupled with a 100 % survival rate. Comparative analysis

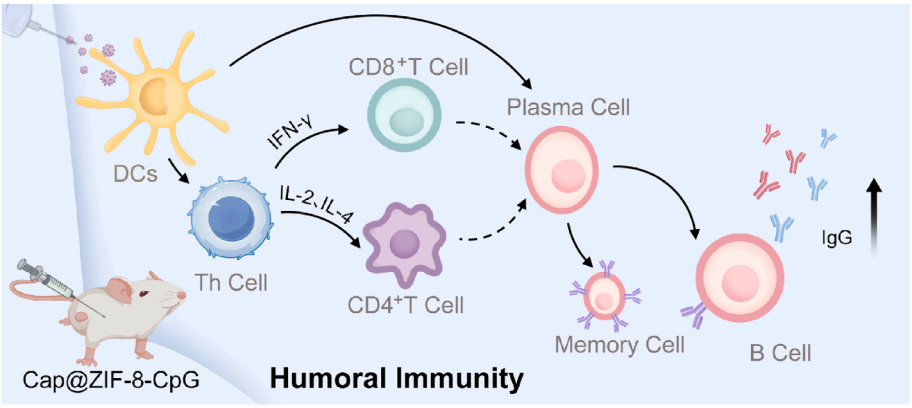

Fig. 8. Schematic of immunity activation by the Cap@ZIF-8-CpG nanovaccine. The dashed-line part in the figure is used to delineate elements not examined in this study. These aspects await further exploration and validation.

indicated that at 14 days postchallenge, mice in the control group experienced more diminished body weight in contrast with the immune groups (Fig. 7a). Remarkably, the Cap@ZIF-8-CpG group exhibited the highest specific antibody titers and superior protection efficacy, as evidenced by the lowest viral loads detected in the spleen and lungs (Fig. 7b–d). Despite the absence of obvious clinical symptoms, the affected organs (spleen and lungs) were histologically assessed, with results revealing pathological alterations such as pulmonary hemorrhage and splenomegaly.

Relative to the Cap@ZIF-8-CpG group, the spleen pathological sections in the control group revealed notable changes. H&E staining results demonstrated an increase in the diameter of the spleen's white pulp, accompanied with slight infiltration of inflammatory cells within splenic nodules. Furthermore, the H&E staining of lung pathological sections exhibited focal necrosis of lymphocytes in the splenic white pulp, accompanied with pulmonary interstitial broadening and hemorrhage (Fig. 7e). Meanwhile, immunohistochemical images were consistent with the abovementioned results. For the control group, they revealed a robust positive signal for PCV2 within the cytoplasm of lung macrophages, where some cytoplasms were observed to be stained yellow. Referring to the spleen immunohistochemical images, weaker positive signals for PCV2 were discernible in the cytoplasm of splenic corpuscle lymphocytes and macrophages (Fig. 7f). Both the pathological sections indicated that the Cap@ZIF-8-CpG nanovaccine group was nearest to the healthy state, demonstrating its robust immune effect in protecting the animals from PCV2 virus infection.

Compared with traditional inactivated and subunit vaccines, the Cap@ZIF-8-CpG complex achieves more efficient antigen presentation and immune activation by nanocarriers (Fig. S14). In addition, the MOF-based platform offers higher stability and tunability, which can better meet diverse immunological requirements. While the Cap@ZIF-8-CpG complex has shown robust immune activation in mouse models, its translation to larger animal models presents significant challenges. The scalability of MOF production must be optimized to facilitate large-scale manufacturing, and comprehensive long-term safety assessments are essential. Future research will be directed towards overcoming these hurdles, thereby accelerating the clinical translation of this platform [53].

3.7. Probable mechanism of Cap@ZIF-8-CpG in vivo

As depicted in Fig. 8, we proposed an immunological model to elucidate the probable mechanism by which the Cap@ZIF-8-CpG vaccine enhances immune responses. Following immunization with the Cap@ZIF-8-CpG vaccine, dendritic cells (DCs) recognize the CpG DNA pathogen-associated molecular patterns in the vaccine via TLR9 and engulf Cap antigens encapsulated in ZIF-8. The internalized Cap antigens are processed by DCs and presented on their surface, priming B cells for differentiation into plasma cells and subsequent IgG antibody production, thereby enhancing humoral immunity. Concurrently, antigen-loaded DCs migrate to lymphoid tissues, activating T helper (Th) cells that differentiate into Th1 or Th2 subsets ($CD4^+$ and $CD8^+$ T cells) under the regulation of co-stimulatory molecules and cytokines. During Th2 differentiation, IL-4 secretion promotes B cell clonal expansion, isotype switching, and the generation of antibody-secreting plasma cells [54]. In Th1 differentiation, IFN-γ production facilitates cytotoxic $CD8^+$ T cell activation [55]. These activated $CD8^+$ T cells enhance B cell antibody affinity maturation through IFN-γ-mediated germinal center modulation, thereby bridging cellular and humoral immunity. This description reveals the complex interactions of various immune components during the Cap@ZIF-8-CpG nanovaccine response.

4. Conclusion

We established an MOF-based delivery system as a nanovaccine for enhancing immune responses. In addition to effortlessly enriching abundant antigens and immunopotentiators, the Cap@ZIF-8-CpG nanovaccine exhibited exceptionally sustained release, antigen protection, thermal stability, satisfactory biosafety, and no damage upon inoculation. The *in vivo* immune experimental results demonstrated that the pH-responsive and antigen-protective properties of Cap@ZIF-8-CpG facilitated the delivery of antigens into APCs, significantly enhancing the secretion of the antibody IgG and the cytokines IFN-γ, IL-2, and IL-4. This led to improved humoral responses, resulting in outstanding performance in PCV2 challenge studies with mice as models. Overall, this study demonstrated the potential of MOF-based delivery systems in enhancing humoral immunity against PCV2. This innovative approach offers considerable advantages over traditional vaccination strategies, providing a new promising direction for the development of effective and long-lasting vaccines against PCV2 and other important pathogens.

CRediT authorship contribution statement

Luo-Gang Ding: Writing – original draft, Data curation, Conceptualization. **Min Shi:** Data curation. **Er-Di Yu:** Formal analysis. **Yu-Lin Xu:** Software. **Yu-Yu Zhang:** Resources. **Xing-Liang Geng:** Resources. **Fei Liu:** Software. **Jian-Da Li:** Resources. **Zhi Chen:** Resources. **Jiang Yu:** Writing – review & editing. **Jia-Qiang Wu:** Writing – review & editing, Supervision.

Declaration of competing interest

The authors declare that they have no known competing financial interests or personal relationships that could have appeared to influence

the work reported in this paper.

Acknowledgments

This study was supported by the National Natural Science Foundation of China (22305145), Natural Science Foundation of Shandong Province (ZR2023QB074), Key Research and Development Project in Shandong Province (2022CXPT010 and 2022TZXD0041), Shandong Province Pig Industrial Technology System (SDAIT-08-01), Taishan Scholars Program, and Agricultural Science and Technology Innovation Project of Shandong Academy of Agricultural Sciences.

Appendix A. Supplementary data

Supplementary data to this article can be found online at https://doi.org/10.1016/j.mtbio.2025.101712.

Data availability

yes

References

[1] G. Zhang, P. Jia, G. Cheng, S. Jiao, L. Ren, S. Ji, T. Hu, H. Liu, Y. Du, Enhanced immune response to inactivated porcine circovirus type 2 (PCV2) vaccine by conjugation of chitosan oligosaccharides, Carbohydr. Polym. 166 (2017) 64–72.
[2] M. Cao, J. Yang, X. Wang, W. Hu, X. Xie, Y. Zhao, M. Liu, Y. Wei, M. Yu, T. Hu, Sophora subprostrate polysaccharide regulates histone acetylation to inhibit inflammation in PCV2-infected murine splenic lymphocytes in vitro and in vivo, Int. J. Biol. Macromol. 191 (2021) 668–678.
[3] S. Zhang, C. Mou, Y. Cao, E. Zhang, Q. Yang, Immune response in piglets orally immunized with recombinant Bacillus subtilis expressing the capsid protein of porcine circovirus type 2, Cell Commun. Signal. 18 (2020) 23.
[4] S. Zhang, L. Wang, L. Wang, N. Yu, Y. Dong, J. Hu, Combined antibody tagged HRP Gold nanoparticle probe for effective PCV2 screening in pig farms, Int. J. Nanomed. 17 (2022) 3361–3369.
[5] Y. Mu, C. Jia, X. Zheng, H. Zhu, X. Zhang, H. Xu, B. Liu, Q. Zhao, E.-M. Zhou, A nanobody-horseradish peroxidase fusion protein-based competitive ELISA for rapid detection of antibodies against porcine circovirus type 2, J. Nanobiotechnol. 19 (2021) 34.
[6] F. Gan, Y. Zhou, G. Qian, D. Huang, L. Hou, D. Liu, X. Chen, T. Wang, P. Jiang, X. Lei, K. Huang, PCV2 infection aggravates ochratoxin A-induced nephrotoxicity via autophagy involving p38 signaling pathway *in vivo* and *in vitro*, Environ. Pollut. 238 (2018) 656–662.
[7] M. Sun, S. Wang, Z. Fang, M. Zhao, Y. Gao, T. An, Y. Tu, H. Wang, X. Cai, A sandwich ELISA for quality control of PCV2 virus-like particles vaccine, Vaccines 10 (2022) 2175.
[8] H. Xue, F. Gan, Z. Zhang, J. Hu, X. Chen, K. Huang, Astragalus polysaccharides inhibits PCV2 replication by inhibiting oxidative stress and blocking NF-κB pathway, Int. J. Biol. Macromol. 81 (2015) 22–30.
[9] B. Luo, S. Wu, W. Zou, Z. Zhang, M. Zhao, S. Shi, Y. Liu, X. Xi, Z. Zeng, W. Liang, Z. Yan, L. Zhang, Label-free immunoassay for porcine circovirus type 2 based on excessively tilted fiber grating modified with staphylococcal protein A, Biosens. Bioelectron. 86 (2016) 1054–1060.
[10] C.J. Gunter, G.L. Regnard, E.P. Rybicki, I.I. Hitzeroth, Immunogenicity of plant-produced porcine circovirus-like particles in mice, Plant Biotechnol. J. 17 (2019) 1751–1759.
[11] C. Meyers, X. Mo, X. Li, B. Yin, J. Deng, K. Tian, A. Yuan, Structural roles of PCV2 capsid protein N-terminus in PCV2 particle assembly and identification of PCV2 type-specific neutralizing epitope, PLoS Pathog. 15 (2019) e1007562.
[12] X.-J. Meng, Porcine circovirus type 2 (PCV2): pathogenesis and interaction with the immune system, Annu. Rev. Anim. Biosci. 1 (2013) 43–64.
[13] E. Fehér, F. Jakab, K. Bányai, Mechanisms of circovirus immunosuppression and pathogenesis with a focus on porcine circovirus 2: a review, Vet. Q. 43 (2023) 1–18.
[14] H. Qiu, M. Sun, N. Wang, S. Zhang, Z. Deng, H. Xu, H. Yang, H. Gu, W. Fang, F. He, Efficacy comparison in cap VLPs of PCV2 and PCV3 as swine vaccine vehicle, Int. J. Biol. Macromol. 278 (2024) 134955.
[15] A. Karuppannan, T. Opriessnig, Porcine circovirus type 2 (PCV2) vaccines in the context of current molecular epidemiology, Viruses 9 (2017) 99.
[16] Y. Fan, L. Guo, W. Hou, C. Guo, W. Zhang, X. Ma, L. Ma, X. Song, The adjuvant activity of epimedium polysaccharide-propolis flavone liposome on enhancing immune responses to inactivated porcine circovirus vaccine in mice, Evid-Based Compl. Alt. 2015 (2015) 1–9.
[17] A. Murthy, Y. Ni, X. Meng, C. Zhang, Production and evaluation of virus-like particles displaying immunogenic epitopes of porcine reproductive and respiratory syndrome virus (PRRSV), Int. J. Mol. Sci. 16 (2015) 8382–8396.
[18] Y.-P. Wang, D. Liu, L.-J. Guo, Q.-H. Tang, Y.-W. Wei, H.-L. Wu, J.-B. Liu, S.-B. Li, L.-P. Huang, C.-M. Liu, Enhanced protective immune response to PCV2 subunit vaccine by co-administration of recombinant porcine IFN-γ in mice, Vaccine 31 (2013) 833–838.
[19] C. Venegas-Vargas, L.P. Taylor, D.L. Foss, T.K. Godbee, R. Philip, M. Bandrick, Cellular and humoral immunity following vaccination with two different PCV2 vaccines (containing PCV2a or PCV2a/PCV2b) and challenge with virulent PCV2d, Vaccine 39 (2021) 5615–5625.
[20] P. Ding, Q. Jin, W. Zhou, Y. Chai, X. Liu, Y. Wang, X. Chen, J. Guo, R. Deng, G. F. Gao, G. Zhang, A universal influenza nanovaccine for "mixing vessel" hosts confers potential ability to block cross-species transmission, Adv. Healthcare Mater. 8 (2019) 1900456.
[21] Y. Sun, J. Zhang, Z. Liu, Y. Zhang, K. Huang, Swine influenza virus infection decreases the protective immune responses of subunit vaccine against porcine circovirus type 2, Front. Microbiol. 12 (2021) 807458.
[22] J. Segalés, Best practice and future challenges for vaccination against porcine circovirus type 2, Expert Rev. Vaccines 14 (2014) 473–487.
[23] S. Meas, K. Chaimongkolnukul, J. Narkpuk, P. Mekvichitsaeng, K. Poomputsa, N. Wanasen, Y.M. Roshorm, Humoral and cellular immune responses induced by bivalent DNA vaccines expressing fusion capsid proteins of porcine circovirus genotypes 2a and 2b, Vaccines 12 (2024) 324.
[24] L. Ju, S.-H. You, M.-A. Lee, U. Jayaramaiah, Y.-J. Jeong, H.-S. Lee, B.-H. Hyun, N. Lee, S.-J. Kang, Selection and evaluation of porcine circovirus (PCV) 2d vaccine strains to protect against currently prevalent PCV2, Vaccines 11 (2023) 1447.
[25] Y.-H. Noh, S.-C. Kim, C.-G. Jeong, S.-C. Lee, D.-U. Lee, I.-J. Yoon, W.-I. Kim, Pathological evaluation of porcine circovirus 2d (PCV2d) strain and comparative evaluation of PCV2d and PCV2b inactivated vaccines against PCV2d infection in a specific pathogen-free (SPF) yucatan miniature pig model, Vaccines 10 (2022) 1469.
[26] Z.-H. Liu, Z.-F. Deng, Y. Lu, W.-H. Fang, F. He, A modular and self-adjuvanted multivalent vaccine platform based on porcine circovirus virus-like nanoparticles, J. Nanobiotechnol. 20 (2022) 493.
[27] A.J. Howarth, Y. Liu, P. Li, Z. Li, T.C. Wang, J.T. Hupp, O.K. Farha, Chemical, thermal and mechanical stabilities of metal-organic frameworks, Nat. Rev. Mater. 1 (2016) 15018.
[28] H.-S. Wang, Metal-organic frameworks for biosensing and bioimaging applications, Coord. Chem. Rev. 349 (2017) 139–155.
[29] A. Bavykina, A. Cadiau, J. Gascon, Porous liquids based on porous cages, metal-organic frameworks and metal organic polyhedra, Coord. Chem. Rev. 386 (2019) 85–95.
[30] A. Wang, M. Walden, R. Ettlinger, F. Kiessling, J.J. Gassensmith, T. Lammers, S. Wuttke, Q. Peña, Biomedical metal-organic framework materials: perspectives and challenges, Adv. Funct. Mater. 34 (2024) 2308589.
[31] P. Wiśniewska, J. Haponiuk, M.R. Saeb, N. Rabiee, S.A. Bencherif, Mitigating metal-organic framework (MOF) toxicity for biomedical applications, Chem. Eng. J. 471 (2023) 144400.
[32] W.H. Choi, B.C. Moon, D.G. Park, J.W. Choi, K.H. Kim, J.S. Shin, M.G. Kim, K. M. Choi, J.K. Kang, Autogenous production and stabilization of highly loaded sub-nanometric particles within multishell hollow metal-organic frameworks and their utilization for high performance in Li-O_2 Batteries, Adv. Sci. 7 (2020) 2000283.
[33] H. Furukawa, N. Ko, Y.B. Go, N. Aratani, S.B. Choi, E. Choi, A.Ö. Yazaydin, R. Q. Snurr, M. O'Keeffe, J. Kim, O.M. Yaghi, Ultrahigh porosity in metal-organic frameworks, Science 329 (2010) 424–428.
[34] A. Terzopoulou, J.D. Nicholas, X.-Z. Chen, B.J. Nelson, S. Pané, J. Puigmartí-Luis, Metal-organic frameworks in motion, Chem. Rev. 120 (2020) 11175–11193.
[35] Z. Shi, Z. Gao, X. Zhuang, X. Si, Z. Huang, Y. Di, S. Ma, Z. Guo, C. Li, N. Jin, L. Huang, M. Tian, W. Song, X. Chen, Dynamic covalent hydrogel as a single-dose vaccine adjuvant for sustained antigen release and significantly elevated humoral immunity, Adv. Funct. Mater. 13 (2024) 2400886.
[36] H. Zhang, J. Zhang, Q. Li, A. Song, H. Tian, J. Wang, Z. Li, Y. Luan, Site-specific MOF-based immunotherapeutic nanoplatforms via synergistic tumor cells-targeted treatment and dendritic cells-targeted immunomodulation, Biomaterials 245 (2020) 119983.
[37] B. Zhang, J. Chen, Z. Zhu, X. Zhang, J. Wang, Advances in immunomodulatory MOFs for biomedical applications, Small 20 (2024) 2307299.
[38] H. Wang, M.-Q. Pan, Y.-F. Wang, C. Chen, J. Xu, Y.-Y. Gao, C.-S. Qi, W. Li, X.-H. Bu, Post-synthetic modifications of MOFs by different bolt ligands for controllable release of cargoes, Chin. Chem. Lett. 35 (2024) 109581.
[39] S.E. Alavi, S.F. Alavi, M. Koohi, A. Raza, H. Ebrahimi Shahmabadi, Nanoparticle-integrated metal-organic frameworks: a revolution in next-generation drug delivery systems, J. Pharm. Investig. 54 (2024) 751–783.
[40] S. Li, L. Tan, X. Meng, Nanoscale metal-organic frameworks: synthesis, biocompatibility, imaging applications, and thermal and dynamic therapy of tumors, Adv. Funct. Mater. 30 (2020) 1908924.
[41] Y. Chen, J. Wei, Y. Chu, P. Zhu, T. Zhang, L. Mao, Y. Gao, L. Chen, F. Yuan, Sonochemical synthesis of γ-CD-MOFs microcapsule for myricetin delivery: study of adsorption mechanism, molecular simulation, solubility, antioxidation, biocompatibility, and *in vitro* digestion, Food Hydrocoll. 147 (2024) 109318.
[42] W. Cao, H. Cao, X. Yi, Y. Zhuang, Development of a simple and high-yielding fed-batch process for the production of porcine circovirus type 2 virus-like particle subunit vaccine, AMB Express 9 (2019) 164.
[43] G. Mutwiri, S. van Drunen Littel-van den Hurk, L.A. Babiuk, Approaches to enhancing immune responses stimulated by CpG oligodeoxynucleotides, Adv. Drug Deliv. Rev. 61 (2009) 226.
[44] H. Zhang, W. Chen, K. Gong, J. Chen, Nanoscale Zeolitic Imidazolate Framework-8 as efficient vehicles for enhanced delivery of CpG oligodeoxynucleotides, ACS Appl. Mater. Interfaces 9 (2017) 31519.

[45] F. Peng, Y. Xiang, H. Wang, Y. Hu, R. Zhou, Y. Hu, Biomimetic assembly of spore@ZIF-8 microspheres for vaccination, Small 18 (2022) 2204011.
[46] X.Y. Chen, A.M. Butt, M.C.I. Mohd Amin, Enhanced paracellular delivery of vaccine by hydrogel microparticles-mediated reversible tight junction opening for effective oral immunization, J. Contr. Release 311 (2019) 50.
[47] K. Zhao, Y. Zhang, X. Zhang, W. Li, C. Shi, C. Guo, C. Dai, Q. Chen, Z. Jin, Y. Zhao, Y. Wang, H. Cui, Preparation and efficacy of newcastle disease virus DNA vaccine encapsulated in chitosan nanoparticles, Int. J. Nanomed. 9 (2014) 389.
[48] Z. Teng, F. Hou, M. Bai, J. Li, J. Wang, J. Wu, J. Ru, M. Ren, S. Sun, H. Guo, Biomineralization of virus-like particles by metal-organic framework nanoparticles enhances the thermostability and immune responses of the vaccines, J. Mater. Chem. B 10 (2022) 2853–2864.
[49] R. Murty, M.K. Bera, I.M. Walton, C. Whetzel, M.R. Prausnitz, K.S. Walton, Interrogating encapsulated protein structure within metal-organic frameworks at elevated temperature, J. Am. Chem. Soc. 145 (2023) 7323–7330.
[50] D. Liu, J. Liu, B. Ma, B. Deng, X. Leng, D. Kong, L. Liu, A simple self-adjuvanting biomimetic nanovaccine self-assembled with the conjugate of phospholipids and nucleotides can induce a strong cancer immunotherapeutic effect, Biomater. Sci-Uk. 9 (2021) 84.
[51] X. Zhong, Y. Zhang, L. Tan, T. Zheng, Y. Hou, X. Hong, G. Du, X. Chen, Y. Zhang, X. Sun, An aluminum adjuvant-integrated nano-MOF as antigen delivery system to induce strong humoral and cellular immune responses, J. Contr. Release 300 (2019) 81–92.
[52] X. Li, C. Pan, C. Li, K. Wang, J. Ye, P. Sun, Y. Guo, J. Wu, H. Wang, L. Zhu, Self-assembled proteinaceous nanoparticles for co-delivery of antigens and cytosine phosphoguanine (CpG) adjuvants: implications for nanovaccines, ACS Appl. Nano Mater. 6 (2023) 7637–7648.
[53] Y. Wang, Y. Hu, Q. He, J. Yan, H. Xiong, N. Wen, S. Cai, D. Peng, Y. Liu, Z. Liu, Metal-Organic Frameworks for virus detection, Biosens. Bioelectron. 169 (2020) 112604.
[54] Y. Yamanishi, K. Miyake, M. Iki, H. Tsutsui, H. Karasuyama, Recent advances in understanding basophil-mediated Th2 immune responses, Immunol. Rev. 278 (2017) 237.
[55] Q. Zuo, T. Li, L. Huang, Z. Liu, W. Xue, Macro-microporous ZIF-8 MOF complexed with lysosomal pH-adjusting hexadecylsulfonylfluoride as tumor vaccine delivery systems for improving anti-tumor cellular immunity, Biomater. Sci. 11 (2023) 5025.